Enhancement of dielectronic recombination in crossed electric and magnetic fields

Victor Klimenko, Lung Ko, and T. F. Gallagher
Department of Physics, University of Virginia, Charlottesville, Virginia 22903, USA
(Received 6 March 2003; published 30 July 2003)

Dielectronic recombination (DR) from a continuum of finite bandwidth in Ba atoms has been studied in electric fields of 0–5 V/cm and magnetic fields of 0–240 G for both $\vec{B}\|\vec{E}$ and $\vec{B}\perp\vec{E}$. In electric fields of $\geqslant$0.1 V/cm, the presence of a perpendicular magnetic field increases the integrated DR rate by up to 60%, with the peak enhancement moving towards higher magnetic fields as the electric field is increased. The general behavior of the enhancement for $\vec{B}\perp\vec{E}$—as well its absence for $\vec{B}\|\vec{E}$ is in agreement with theoretical expectations. A simple model is presented to provide insight into the results, and reasons for its shortcomings are presented.

DOI: 10.1103/PhysRevA.68.012723 PACS number(s): 34.80.Lx

I. INTRODUCTION

Dielectronic recombination (DR), the recombination of an ion and an electron via a doubly excited autoionizing state, is the dominant recombination path for the energetic electrons found in a high-temperature laboratory and astrophysical plasmas. Excitation of two electrons in an atom X can give a state X^{**} with an excitation energy $W(X^{**})$ which is higher than the lowest ionization energy of X, i.e., the ground state of X^+. The process in which X^{**} undergoes a radiationless transition to the continuum,

$$X^{**}\rightarrow X^+ + e^-, \tag{1}$$

is known as autoionization. The inverse process in which a radiationless capture,

$$X^+ + e^- \rightarrow X^{**}, \tag{2}$$

is followed by emission of radiation to give a stable singly excited state X^*,

$$X^{**}\rightarrow X^* + h\nu, \tag{3}$$

was first referred to as dielectronic recombination by Massey and Bates [1] in their studies of the ionosphere. Later, the interest in DR arose again in connection with the studies of solar corona, where DR was found to be the dominant recombination process for nonhydrogenic impurity ions. It was pointed out by Burgess [2] that for sufficiently highly excited states, collisional processes that are faster than radiative decay to lower states can alter the DR rates from what might be expected in an otherwise collisionless environment. Burgess and Summers [3] were first to suggest that the DR rate could be enhanced by the effects of collisionally induced angular-momentum l redistribution of the doubly excited states.

It is a straightforward matter to give a quantitative description of DR for the case in which a ground-state ion collides with an electron to form a doubly excited state converging to the first excited state of the ion. DR is somewhat more complex when more than two ionic levels are considered, but the essential ideas are unchanged.

The first step of the DR process, the capture, is simply the inverse of the autoionization process, and therefore, by the principle of detailed balance, may be characterized by the autoionization rate. The DR rate Γ_{nl} through a nl state converging to the first excited state of the ion is the product of the electron-capture rate into the nl state and the branching ratio for radiative decay to the bound state:

$$\Gamma_{nl}=\beta A_{nl}\frac{A_R}{A_{nl}+A_R}\approx\beta A_<. \tag{4}$$

Here, A_{nl} is the autoionization rate of the nl state, β is a constant, A_R is the radiative decay rate (also a constant independent of n and l), and $A_<$ is the lesser of A_R and A_{nl}. A_{nl} falls off as $1/n^3$ and rapidly with l, so in a field-free collisionless environment only low-n, low-l states have a sizable contribution to DR. For these states $A_{nl}>A_R$, and therefore $\Gamma_{nl}=\beta A_R$. This means that each of these states makes the same contribution, $\Gamma_{nl}=\beta A_R$, to the total DR rate—so a reasonable estimate of the total, energy integrated, DR rate Γ is obtained by simply counting these states: $\Gamma=\beta N A_R$. If the low-l character can be redistributed in any way over higher-l states, to raise their autoionization rates, then more states are involved in the process, opening more paths for recombination and thus increasing the DR rate. The fact that the total rate can be estimated by simply counting states ensures that the Rydberg states play a central role in DR. Since Rydberg states are easily perturbed, it is not surprising that small external perturbations have significant effects on the DR rates.

In a plasma collisions with ions and electrons are such perturbations. To a reasonable approximation, a collision with a charged particle is equivalent to exposure to an electric-field pulse. Due to their respective masses, collisions with ions and electrons resemble quasistatic and high-frequency electric fields, respectively. The notion that the ions would enhance DR due to Stark l mixing by their (quasi-)static electric field was introduced by Jacobs, Davis, and Kepple [4]. They found that the electric fields can induce DR through the normally inaccessible high-l states by converting them to Stark states. The measurements of DR performed by Belić *et al.* [5] using crossed Mg^+ and e^- beams provided the first direct measurements of DR. However, the measured DR cross sections turned out to be several times larger than the theoretical ones. The agreement between theory and experiment was much improved after LaGattuta

and Hahn [6] took into account the presence of the motional electric field in the experiment of Belić *et al.* [5]. Müller *et al.* [7] gave the first experimental confirmation of the enhancement of DR as a function of the electric field in the collision region. Since then many other DR experiments using different techniques, such as storage rings (Bartsch *et al.* [8]), have been performed, and the two effects of static or quasistatic electric fields on DR have been shown to be as predicted by Jacobs, Davis, and Kepple [4] and are by now reasonably well understood: (a) mixing of the l states creates Stark states, which increases the DR rate and (b) depression of the ionization limit lowers the DR rate. The state mixing is reasonably well described by a hydrogenic picture [9]. The E field couples the degenerate l states of the same n and m, converting them to nkm Stark states with the same n and m. Each of the Stark states contains low-l character and, to a reasonable approximation, has the average autoionization rate of all contributing l states of the same n and m. This rate typically exceeds A_R, so the effect of the field is to convert the high-l states to Stark states which contribute to the DR rate—i.e., the high-l states, which in zero field have $A_{nl} < A_R$, are converted into Stark states which have ionization rates $A_{nk} > A_R$. In essence, the previously wasted high autoionization rates of the low-l states are shared with the high-l states. This phenomenon was explicitly observed by Safinya, Delpech, and Gallagher [10] and Jaffe *et al.* [11].

Magnetic fields were long ignored, with the exception of the work by Huber and Bottcher [12], who pointed out that, in very strong magnetic fields, the diamagnetic term can also cause mixing of l states. Recently, the interest in magnetic fields arose again in connection with the crossed-beam and storage-ring DR experiments, in which a magnetic field is necessary to separate the recombination products. In a number of measurements, the experimentally measured DR rates were well above the theoretical calculations (see, for example, Refs. [8,13,14]), indicating that there might be additional enhancement of DR beyond that due to the electric-field l mixing. In response to this, Robicheaux and Pindzola [15], Griffin, Robicheaux, and Pindzola [16], and LaGattuta and Borca [17] performed model calculations of DR in the presence of crossed electric and magnetic fields. They suggested that if the magnetic field has a component that is perpendicular to the electric field, states with different magnetic quantum numbers m are mixed, since, unlike the case in an electric field alone, m is no longer a good quantum number, and this mixing opens more recombination channels, i.e., the former high-m states. An electric field alone does not mix m states, so high-m states still do not contribute to DR in an electric field.

In contrast to an electric field, a B field alone does not alter the DR rate, unless it is so strong as to produce l mixing [10]. However, when combined with an E field, the B field can have an effect. As pointed out by Robicheaux and Pindzola [13], a magnetic field perpendicular to the electric field creates states which are mixtures of m states, and by this mixing the high-m states can be given high enough autoionization rates to contribute to DR. To understand, at least qualitatively, how the effect arises let us imagine that we apply first an E field, then add the B field. For $\vec{B} \| \vec{E}$, there is no effect of the B field since neither field couples states of different m, and the B field simply shifts Stark states of different m relative to each other. If $\vec{B} \perp \vec{E}$, the B field couples Stark states of m and $m \pm 1$. This coupling of the m states can be expected to raise the DR rate because high-m states are now coupled to low-m states, which raises the autoionization rates of the high-m states. In essence, the B field leads to an m mixing analogous to the l mixing produced by an electric field. For B fields low enough that diamagnetism can be neglected we would expect a magnetic field parallel to the electric field to have no effect. The more general case in which the angle between E and B is not 0° or 90° has been examined by LaGattuta and Borca [15], who calculated DR rates for $Mg^+ + e^-$ and found a nontrivial dependence on the angle between $\vec{E}$ and $\vec{B}$ [15].

The recent storage-ring DR measurements by Bartsch *et al.* [18,19] on Li-like Cl^{14+} and Ti^{19+} ions were the first ''intentional'' measurements of DR in crossed E and B fields. The authors did observe that a magnetic field altered the DR rate. However, as the magnetic field increased from 200 to 690 G, the DR rate decreased, contrary to what one might expect on the basis of the above discussion. In our previous work [20] on DR from a continuum of finite bandwidth (CFB) [21] in Ba atoms, we demonstrated that DR was indeed enhanced in crossed electric and magnetic fields. Here, we present a more systematic study of DR in electric fields of 0–5 V/cm and magnetic fields of 0–240 G. In these measurements, we are able to enter a regime in which the magnetic field is relatively high and the magnetic field enhancement begins to decrease with increasing B. We describe our experimental approach in Sec. II and present our results in Sec. III. In Sec. IV, we present a simple physical model describing the effects of crossed E and B fields on DR. We compare our results and the storage-ring results to this model and suggest why the observations deviate from the predictions of the model in some cases.

II. EXPERIMENTAL APPROACH

The essential notion of a CFB is most easily understood by considering our experiments with Ba. As shown by Fig. 1, the CFB is the broad autoionizing $6p_{3/2}11d$ state which straddles the Ba^+ $6p_{1/2}$ limit. We excite Ba atoms from the ground state to a well-defined energy in the CFB using three laser pulses via the route $6s^2 \rightarrow 6s6p \rightarrow 6s11d \rightarrow 6p_{3/2}11d$. In a classical view of the $6p_{3/2}11d$ state, the outer $11d$ electron makes roughly 20 orbits before it is inelastically scattered by the Ba^+ $6p_{3/2}$ core and autoionizes. If the electron induces the Ba^+ $6p_{3/2} \rightarrow 6s_{1/2}$ dipole transition, autoionization occurs, while if it induces the Ba^+ $6p_{3/2} \rightarrow 6p_{1/2}$ quadrupole transition, it is captured into the degenerate $6p_{1/2}nd(ns)$ state. Once in the $6p_{1/2}nd(ns)$ state the atom can either autoionize, directly or via the $6p_{3/2}11d$ state, or radiatively decay to the bound $6s_{1/2}nd(ns)$ state. The latter completes DR, and we detect by field ionization those atoms which have radiatively decayed to the bound $6s_{1/2}nl$ states.

There is a difference between our experiment and true DR. In our experiment, the incoming electron is a d wave of

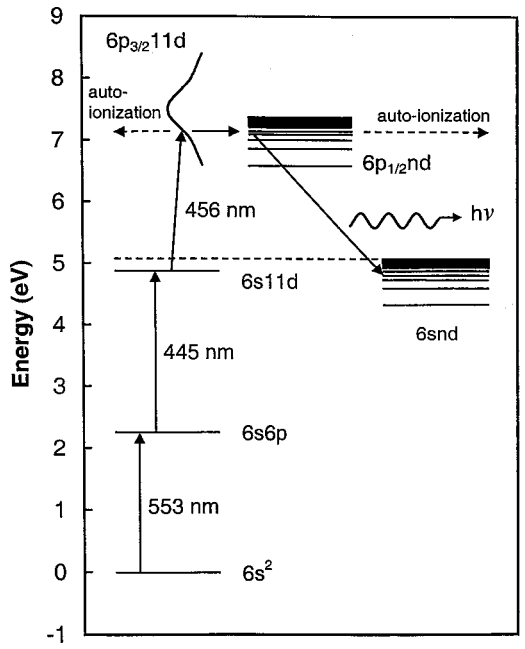

FIG. 1. Ba energy-level diagram. Three dye lasers are used to drive the transitions from the Ba $6s^2$ ground state to the $6p_{3/2}11d$ state, the continuum of finite bandwidth. From the continuum of finite bandwidth, the $11d$ electron can either autoionize into the true continuum or be captured into the degenerate $6p_{1/2}nd$ state, as shown by the two horizontal arrows from the $6p_{3/2}nd$ state. If capture occurs, the $6p_{1/2}nd$ state can either autoionize or decay radiatively to the bound $6snd$ state as shown by the wavy arrow. In the latter case, dielectronic recombination has occurred, which we detect by field ionization of the bound $6snd$ Rydberg state.

known m, while in true DR all partial waves are present. Since low-m states are expected to contribute much of the true DR rate, we do not expect this difference to be particularly significant especially since the rate of DR from a CFB can be described by an equation of the same form as the one describing true DR [22], and this description gives a faithful representation of the experimental results [23]. However, as we shall see, a noticeable difference between our experiment and the storage-ring experiments arises from the fact that we have only a d entrance channel instead of all ℓ states.

A general discussion of the experimental techniques used in this work and the theoretical background for autoionizing Rydberg states can be found elsewhere [24]. The experimental arrangement that we used includes the vacuum chamber, which contains the interaction-region assembly and is typically maintained at a pressure of $\sim 10^{-7}$ Torr, and the optical system, which includes a commercial 20-Hz repetition rate pulsed Nd:YAG (yttrium aluminum garnet) laser and three custom-built Littman dye lasers [25]. The first two dye lasers (pumped by the second and third Nd:YAG laser harmonics, respectively) are fixed in frequency to drive the Ba $6s^2 \rightarrow 6s6p$ and $6s6p \rightarrow 6s11d$ transitions at 553 and 445 nm, as shown in Fig. 1. The third laser (pumped by the third harmonic) is used to drive the $6s11d \rightarrow 6p_{3/2}11d$ transition at ~456 nm, and its frequency is scanned by a computer-controlled stepping motor to vary the initial energy of the electron in the CFB. The dye laser pulses have a

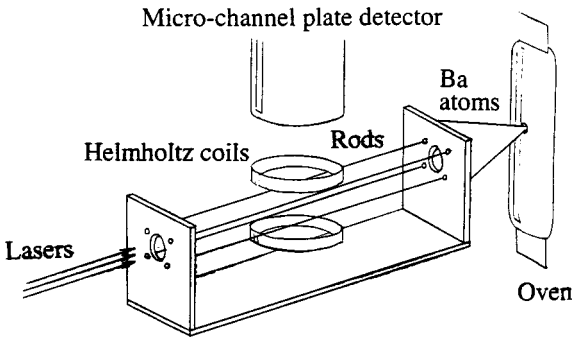

FIG. 2. Interaction region assembly.

~ 0.2–0.5 cm^{-1} bandwidth and are about 5 ns long. All three dye lasers are vertically polarized to ensure the excitation of $m=0$ states only. The vacuum chamber is a hollow aluminum ''drum'' that has a quartz window to provide optical access to the interaction region. Inside the chamber is a resistively heated oven that emits a thermal beam of Ba atoms through a ~0.5-mm-diameter hole when a current is passed through it. The thermal beam of Ba enters the interaction region, where the atoms are excited by the dye laser pulses. The laser excitation occurs in the presence of the external fields. Approximately 200 ns after the excitation, the recombined atoms are ionized by an electric-field pulse (with the rise time of ~ 1 μs that drives the field-ionized electrons into a microchannel-plate detector, producing a signal proportional to the number of atoms that underwent DR. This signal is captured using a gated integrator and recorded in a computer.

The interaction-region assembly is shown in Fig. 2. An atomic beam passes down the axis of four brass rods. The 0.24-cm-diameter rods are 1.00 cm apart vertically and horizontally. By applying voltages to the upper and lower pairs or to the left and right pairs, we can produce horizontal or vertical E fields. The magnetic field is created by a pair of Helmholtz coils. The vertical axis of the coils goes through the interaction region. The coils have 54 turns, are 2.54 cm in radius, and are 2.54 cm apart ($R=d$ is the condition that gives an approximately uniform magnetic field on the axis of the coils). The three laser beams are counterpropagating to the atomic beam along the axis of the four rods.

The E and B fields used in the experiment are pulsed. The magnetic field is produced by discharging a 5 μF capacitor through the Helmholtz coils, producing a current pulse 100 μs long. The highest voltage available to charge the capacitor is 320 V, which results in a peak current of 14.7 A and a peak magnetic field of 240 G, the maximum field used in the experiment. The laser is fired at the peak of the magnetic-field pulse. The magnetic field is calibrated using a gaussmeter. The presence of a vertical magnetic field slightly increases the detected electron signal (compared to the $B=0$ case), since the trajectories of the field-ionization electrons are forced to spiral around the magnetic field, which prevents a natural loss of some of them from the interaction region. To measure this increase in signal we excite the bound $6snd$ states in the high-n region ($n \sim 150$), where the n states are not resolved and the excitation spectrum is relatively flat. By measuring the signal level with and without the B field, we establish the *collection-efficiency* factor

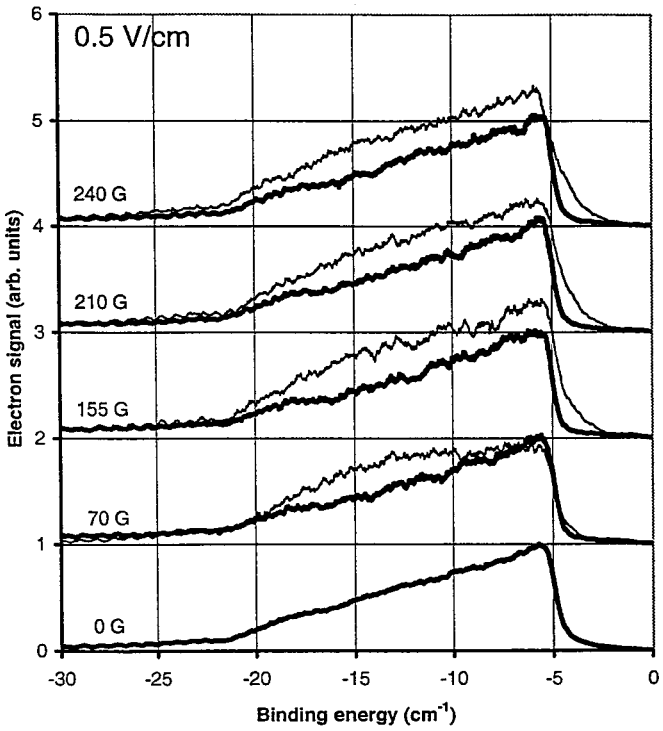

FIG. 3. The DR signal obtained by scanning the frequency of the third laser in $E=0.5$ V/cm electric field and $B=(0-240)$ G magnetic field, with $\vec{B}\|\vec{E}$ (bold line) and $\vec{B}\perp\vec{E}$ (thin line). The energy scale is relative to the Ba^+ $6p_{1/2}$ limit.

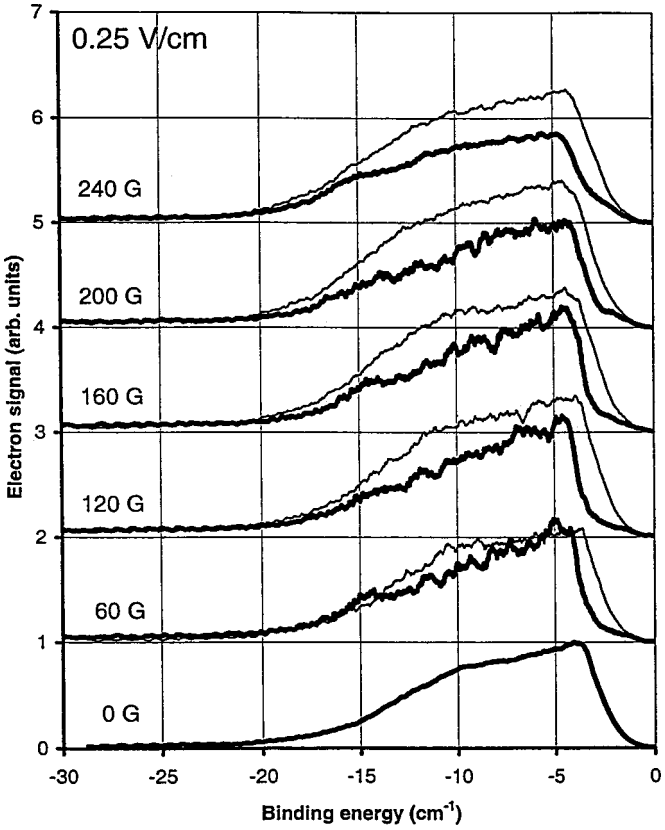

FIG. 4. Same as Fig. 3 for $E=0.25$ V/cm.

$$\gamma=\frac{\mathcal{S}(B)}{\mathcal{S}(0)}=1+4.70\times10^{-4}B+2.45\times10^{-6}B^2, \qquad (5)$$

where $\mathcal{S}$ is the signal and B is in gauss. This factor is used to correct the experimental data taken with $B\neq0$. It is a 25% correction at the highest field we used. We estimate the uncertainty of the collection efficiency factor to be 20%. The laser excitation shown in Fig. 1 occurs in a vertical or horizontal E field, which is provided by a 5-μs voltage pulse straddling the laser pulses applied to the vertically or horizontally opposing pairs of rods shown in Fig. 1. Roughly, 100 ns after the laser pulses, we apply a negative voltage pulse to the lower pair of rods to provide a 100-V/cm field-ionization pulse. To allow the application of a field-ionization pulse perpendicular to the 5 μs pulse we have used a resistor-diode network.

III. RESULTS

In Fig. 3, we show a sample series of DR signals recorded by scanning the frequency of the third laser of Fig. 1, with $E=0.5$ V/cm and B varied from 0 to 240 G, for $\vec{B}\|\vec{E}$ and $\vec{B}\perp\vec{E}$. $E=0.5$ V/cm is chosen because the energy-integrated DR rate in an E field alone attains its maximum at this value [21]. The energy scale is relative to the Ba^+ $6p_{1/2}$ limit. When $\vec{B}\|\vec{E}$, the data (corrected by the collection-efficiency factor γ) are nearly identical to the $B=0$ data, proving that adding the parallel B field does nothing, as expected, since adding the B field does not change the symmetry and mix m states. It is quite apparent in Fig. 3 that there is a clear difference between $\vec{B}\perp\vec{E}$ and $\vec{B}\|\vec{E}$ and that $\vec{B}\perp\vec{E}$ produces an obvious enhancement of the DR rate.

Other values of the electric field were examined as well. The representative series of scans taken with $E=0.25$ V/cm (Fig. 4), $E=1$ V/cm (Fig. 5), and $E=2$ V/cm (Fig. 6) support the observation made for $E=0.5$ V/cm. Once again, as the B field is varied from 0 to 240 G, the $\vec{B}\|\vec{E}$ γ-corrected data exhibit only marginal, if any, increase of DR signal, remaining almost identical to the $B=0$ data, while the $\vec{B}\perp\vec{E}$ data show a clear DR enhancement. Finally, Figs. 7 and 8 show the typical data series for the smallest and the largest E fields used in the experiment, 0.1 and 5 V/cm, respectively, with $\vec{B}\perp\vec{E}$ and $\vec{B}\|\vec{E}$ (where available). The 5 V/cm $\vec{B}\|\vec{E}$ data series shows a slight decrease of DR signal when the magnetic field goes up. However, as before, there is a clear difference between $\vec{B}\perp\vec{E}$ and $\vec{B}\|\vec{E}$, with the $\vec{B}\perp\vec{E}$ data showing an obvious enhancement of DR.

The data shown in Figs. 3–8 show clearly the energy resolved enhancement of DR for $\vec{B}\perp\vec{E}$ and lack of enhancement for $\vec{B}\|\vec{E}$. To obtain a quantitative value for the enhancement of the energy integrated DR signal, we integrate the DR signal $S(B,E,W)$ for a given B and E, such as those of Figs. 3–8, over binding energy W, and define a magnetic-field enhancement factor

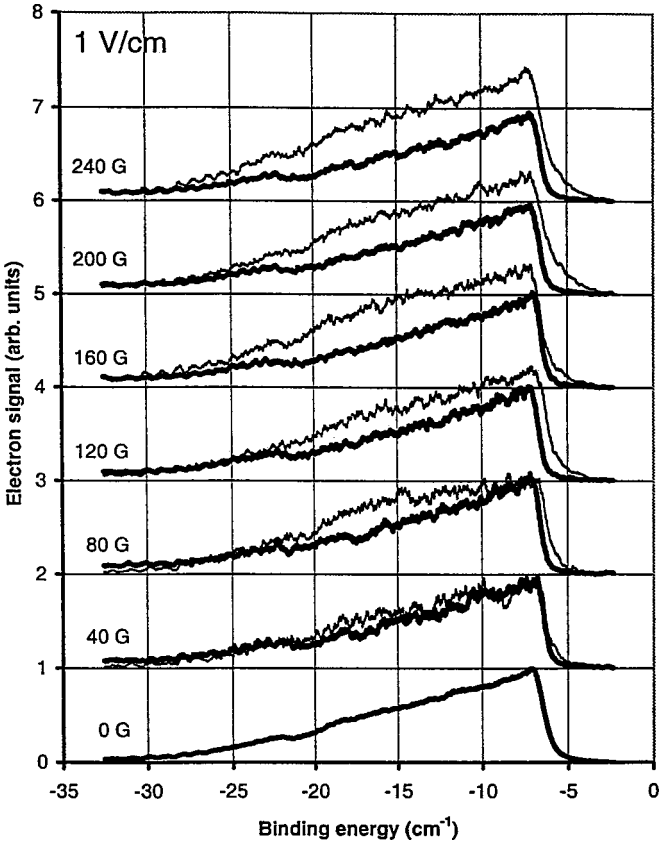

FIG. 5. Same as Fig. 3 for $E=1.0$ V/cm.

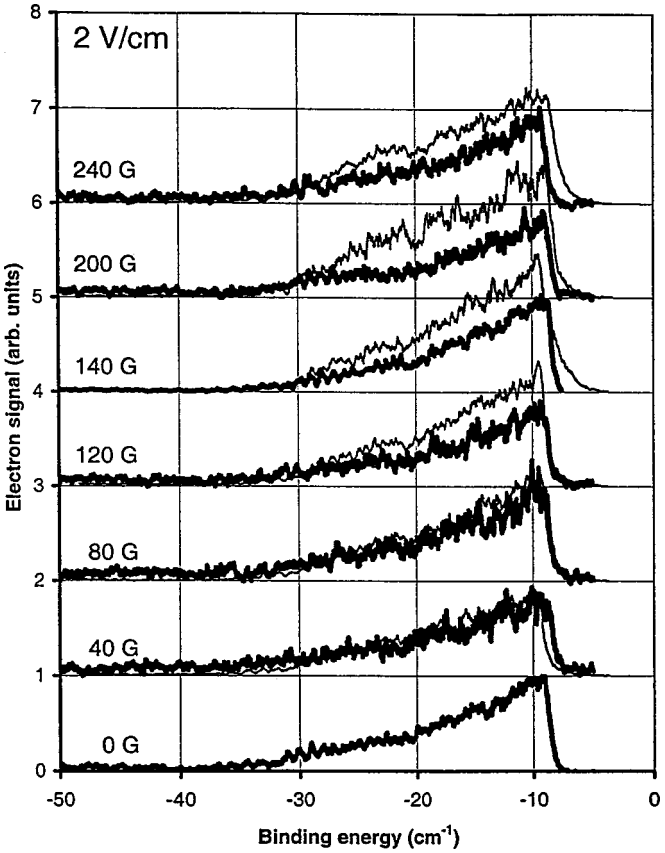

FIG. 6. Same as Fig. 3 for $E=2.0$ V/cm.

$$R(\vec{B},\vec{E})=\frac{\int S(\vec{B},\vec{E},W)dW}{\int S(0,\vec{E},W)dW}. \tag{6}$$

By repeating the scans leading to Figs. 3–8 for different combinations of B and E fields, we can determine the B and E dependence of $R(B,E)$, and in Fig. 9 we show plots of $R(\vec{B}\|\vec{E})$ and $R(\vec{B}\perp\vec{E})$ as a function of B for all six values of electric field used in the experiment. Each point in Fig. 9 corresponds to a trace analogous to the ones shown in Figs. 3–8.

In Fig. 9, the experimental $R(B,E)$ values are fit to third-order polynomials in B to show the trends. In all cases there is only marginal, if any, enhancement with $\vec{B}\|\vec{E}$ and a substantial enhancement with $\vec{B}\perp\vec{E}$. In particular, adding the perpendicular magnetic field enhances the DR rate, by as much as a factor of 1.4–1.6, which is consistent with the calculations of Robicheaux and Pindzola [15] who obtained a (30–50)% enhancement for a realistic atomic model. Also in agreement with the calculations, and equally important, the enhancement factor appears to reach a maximum and declines as the B field is further increased for the lower values of E.

Our $\vec{B}\perp\vec{E}$ DR enhancement data are summarized in Table I.

It is useful to summarize the factors that may have affected the experimental data presented in this section.

(1) The decrease of the DR signal in parallel fields, clear in $E=0.1$ and 5 V/cm fields (Figs. 7 and 8) and also seen in $E=0.25$ V/cm (Fig. 4) and $E=2$ V/cm (Fig. 6) data, is, most likely, an artifact caused by the correction for the collection-efficiency factor γ. The data assembled to calculate γ were taken under differing experimental conditions. Experimental parameters, such as the oven current, tend to drift from series to series and sometimes from scan to scan, while the dye laser alignment tends to drift in time, decreasing the signal level. The location of the interaction spot is subjectively determined by the experimenter, who manually adjusts the laser beams to achieve the maximum zero-field signal. This last factor is important because the E and B fields created by a four-rod configuration and Helmholtz coils, respectively, are only *approximately* uniform within the interaction-spot area—so, on a given day, the interaction spot may be exposed to slightly different E and B fields. Stray fields present in the vacuum chamber also have an unpredictable nature and may change on day-to-day basis. Most likely, variations in all these factors average out to some extent in the collection-efficiency factor γ. However, the experimental conditions for each particular DR signal scan or series of scans are inevitably different from the average conditions, leading to an overcorrection or undercorrection of the data by γ.

(2) With stray electric fields of up to 0.2 V/cm present in the vacuum chamber it is, of course, nearly impossible to

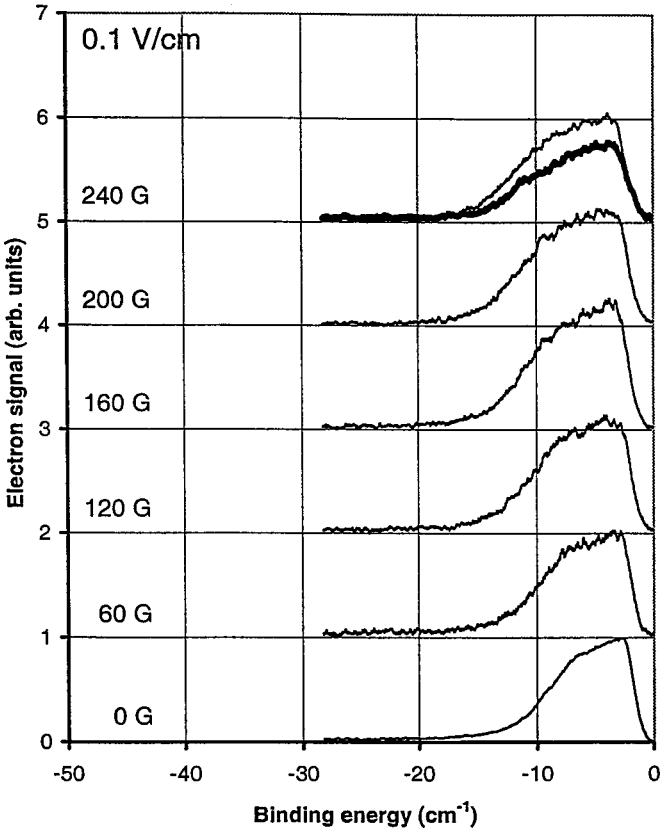

FIG. 7. Same as Fig. 3 for $E=0.1$ V/cm.

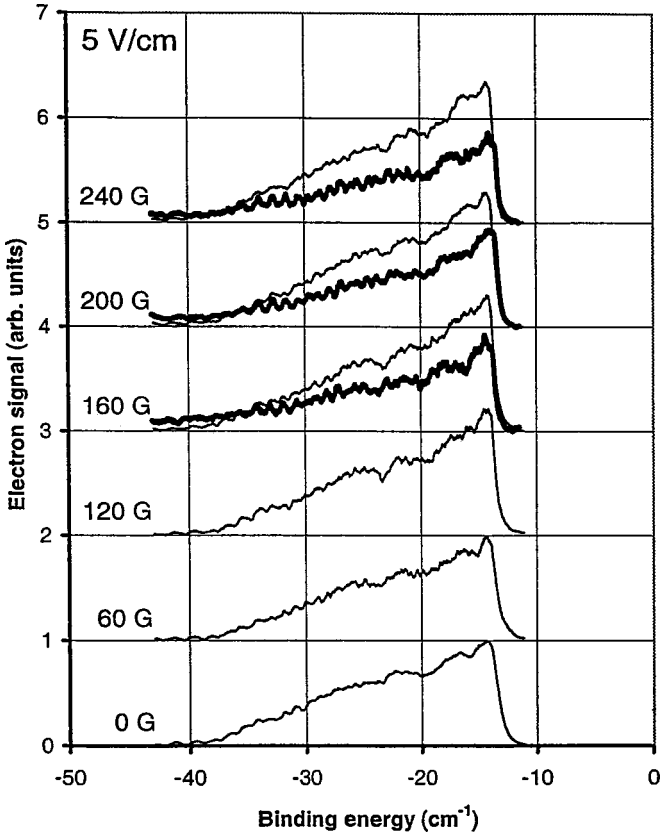

FIG. 8. Same as Fig. 3 for $E=5.0$ V/cm.

ensure that the $\vec{E}$ field is *exactly* parallel or perpendicular to the B field. This may be an additional reason why the $\vec{B}\|\vec{E}$ data—for example, the $E=0.25$ V/cm data (Fig. 4)—exhibit a slight enhancement of DR as the magnetic field goes up. The 0.25 V/cm $\vec{B}\|\vec{E}$ enhancement curve (see Fig. 10) appears to "mimic" the $\vec{B}\perp\vec{E}$ enhancement curve, further suggesting that the fields were not perfectly parallel.

(3) With our thermal beam, the problem of the motional $\vec{E}=\vec{v}\times\vec{B}$ field is substantially reduced from the storage-ring experiments [18,19], but it is still present. For the highest B field, we used, 240 G, the perpendicular motional E field, 80 mV/cm, at the peak of the velocity distribution of the atomic beam. This field is oriented in the direction opposite to the perpendicular E field which we apply and at the lowest applied fields where we can see its effect. For example, in the $E=0.25$ V/cm data the ionization threshold for $\vec{E}\perp\vec{B}$ is at a higher energy than for $\vec{E}\|\vec{B}$. At several times, we measured the electric-field ionization threshold for the $\vec{B}\perp\vec{E}$ case with the E field reversed and it moved to higher energy for the same applied field. However, the change was comparable to the uncontrolled variations in the stray field. Consequently, rather than explicitly correcting our data for the presence of the motional field, we have chosen to point out its presence as well as the presence of stray electric fields of comparable magnitude.

The factors discussed above, though leading in some cases to a substantial spread of the enhancement data points, do not affect the most important features and trends that are clearly seen in the data presented. We estimate the statistical uncertainty of the magnetic field enhancement factor to be 20%.

IV. DISCUSSION

To date there have been two sets of experiments on DR in combined electric and magnetic fields, and they appear to give contradictory results. Specifically, in the storage-ring experiments DR decreases with increasing magnetic field, while in our experiments with the continuum of finite bandwidth it generally increases with magnetic field. Before considering the case of combined E and B fields, it is useful to return to the pure electric field case, in which there are also clear differences between the two types of experiments. In the storage-ring experiments, the energy resolved DR signal increases with applied electric field for all energies, and in our experiments it does not; it saturates quickly with E field and goes to zero above the classical field ionization limit. In this section, we first briefly review why the two experiments are different in a pure electric field, which sets the stage for understanding the combined field case. To understand the combined E and B field case, we introduce a simple model which reproduces the central results of the experiments and the more involved numerical calculations.

We begin by considering the effect of an E field alone, and in Fig. 10 we show the energy-level diagram for a Rydberg electron bound to an ion of charge Z. We assume that the $\ell=0$ state has a nonzero quantum defect δ and all the

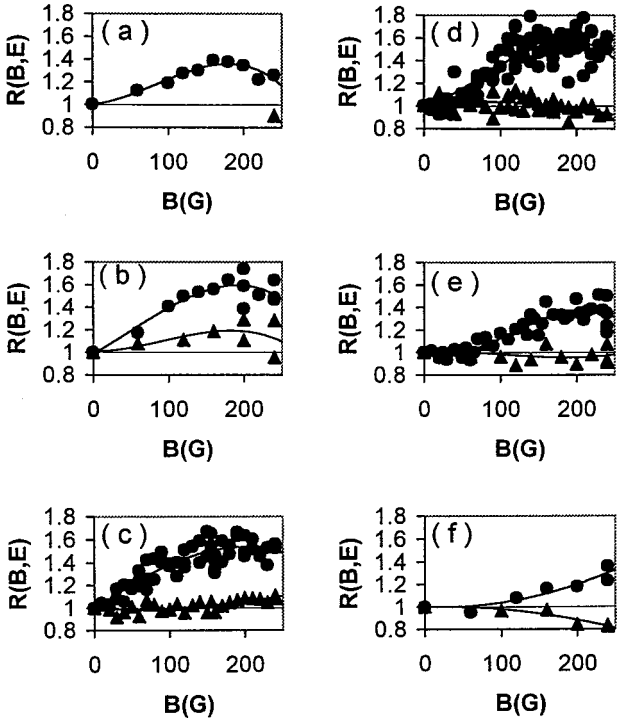

FIG. 9. The magnetic-field enhancement factor $R(B,E)$, the ratio of the energy-integrated DR rate with and without the B field [see Eq. (7)] vs B, for $\vec{B}\|\vec{E}$ (filled triangles) and $\vec{B}\perp\vec{E}$ (filled circles). (a) $E=0.1$ V/cm, (b) $E=0.25$ V/cm, (c) $E=0.5$ V/cm, (d) $E=1.0$ V/cm, (e) $E=2.0$ V/cm, (f) $E=5.0$ V/cm. Solid lines are fits of $R(B,E)$ to third-order polynomials.

others are hydrogenic ($\delta=0$). The natural field scale for the problem is the Inglis-Teller field $E_{\rm IT}$ defined by

$$E_{\rm IT}=\frac{Z^3}{3n^5}, \tag{7}$$

which is the field at which the extreme n and $n+1$ Stark states of $m=0$ intersect as shown by Fig. 10. Adjacent hydrogenic Stark states of the same m are separated by $\Delta W=3nE/Z$, and states of $m\pm1$ are interleaved with the $m=0$ states so that the spacing of states differing by one in m is $\Delta W=3nE/2Z$. If we ignore the Stark shift of an $m=0$ state with $\delta\neq0$, it joins the Stark manifold at the field

$$E_\delta=2\,\delta E_{\rm IT}, \tag{8}$$

TABLE I. Magnetic fields for maximum enhancement and maximum enhancement factors.

Electric field (V/cm)	Enhancement maximum position (G)	Peak enhancement factor
0.1	178	1.36
0.25	192	1.60
0.5	198	1.54
1.0	190	1.58
2.0	210	1.38
5.0	>240	1.3

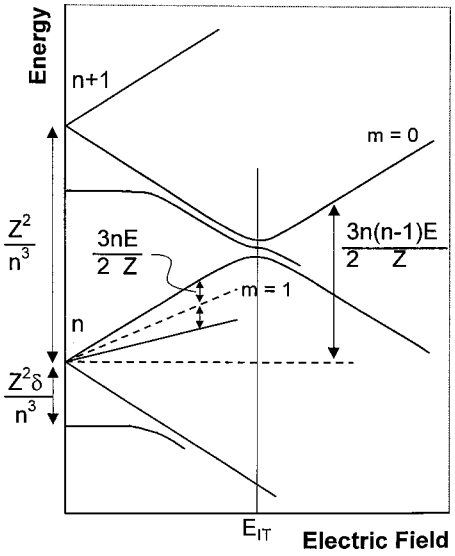

FIG. 10. Energies for selected $m=0$ states in an electric field (—) for an atom which has ns states with nonzero quantum defect and all higher-ℓ states with quantum defects of zero. The n and $n+1$ levels intersect at the Inglis-Teller field $E_{\rm IT}=Z^3/3n^5$, and the ns states join the Stark manifold and the field $E=2\,\delta E_{\rm IT}$. Finally, the $m=1$ states (– – –) lie midway between the $m=0$ states.

as shown in Fig. 10. While in Fig. 10, we have shown one state having $\delta\neq0$, in practice, in any nonhydrogenic atom, all states have nonzero quantum defects, and for high ℓ they originate in the dipole polarizability α_d of the core. Explicitly, the quantum defect of the $n\ell$ state is given by [24]

$$\delta_\ell=\frac{n^3\alpha_d}{2}\langle r^{-4}\rangle, \tag{9}$$

which for high ℓ is approximately given by [24]

$$\delta_\ell=\frac{3\alpha_d}{4\ell^5}. \tag{10}$$

Consequently, in any nonhydrogenic atom, for a given value of n, as the electric field is raised progressively lower ℓ states join the Stark manifold. An ℓ state joins the manifold when the field given by Eq. (8) is reached for its quantum defect. In the storage-ring experiments, electrons were combined with Li-like ions to give Be-like ions. In Be the $2snf$ states have a quantum defect of 0.033 [26], and since quantum defects are independent of Z, we can use this quantum defect for $\ell=3$ to determine α_d in Eq. (9), which in turn allows us to relate quantum defects to ℓ.

Using the picture above, we can compare how an electric-field affects the storage ring and continuum of finite bandwidth DR experiments. The storage-ring experiment with Si^{11+} was carried out in E fields of up to 181 V/cm [27], which is far below the Inglis-Teller field for the n range of importance, and only relatively high-ℓ states are affected by the field. DR of electrons with energy <18 eV is unaffected by the applied E field. These electrons correspond to states of $n\leqslant20$ converging to the $2p_{1/2}$ limit. For $n=20$ and $Z=11$, $E_{\rm IT}=7.12\times10^5$ V/cm, and using Eq. (8), we can conclude

that in zero field at $n=20$ only states with $\delta>1.3\times10^{-4}$ or $\ell>10$ are Stark mixed by the field. Since the field does not produce an increase in the DR rate, we infer that the zero-field autoionization rates of the $\ell>10$ states are all less than the radiative decay rate. Consequently, $\ell\leqslant10$ states must be the major contributors to the DR rate. The peak DR signal occurs for incoming electrons with 22.2 eV of energy. They are captured into states bound by roughly 0.9 eV relative to the $2p_{1/2}$ limit, i.e., $n=43$. In this case, at 181 V/cm $E_{\mathrm{IT}}=1.55\times10^{4}$ V/cm, and applying Eq. (8), we see that states with $\delta\leqslant6\times10^{-3}$ are part of the Stark manifold. So the electric-field enhancement comes from mixing the $\ell=5-10$ states with the higher-ℓ states. For $n\leqslant43$, the $\ell<5$ states are not affected by the E field, and these states are not part of the Stark manifold. If the field were raised above 181 V/cm, we expect that the DR rate would continue to rise until all ℓ states were admixed to the Stark manifold, at a field of $E\approx E_{\mathrm{IT}}$.

In sum for a given n, we can expect a monotonic increase in the DR rate with E because progressively lower-ℓ states are admixed to the Stark manifold. Since decreasing ℓ leads to a larger capture rate, the increase of the DR rate with E is dramatic. Finally, we note that the observed DR signal is artificially cutoff at $n=47$ by the motional E field from a downstream magnet, so the expected depression of the limit by the applied field in the recombination region does not appear in the data.

It is interesting to note that the importance of high-ℓ states in DR of Pb^{79+} has been suggested in the report of a recent experiment on DR of Pb^{79+} [28]. Specifically, the calculated DR rates show that states of up to $\ell\approx15$ are important. As we have just shown, the E field dependence of DR in Si^{11+} shows, in an experimental way, the importance of states of ℓ as high as ten.

Our experiments with the continuum of finite bandwidth differ significantly from the storage-ring experiments in that the entrance channel contains only the Ba $6p_{1/2}$ *nd* states, not all ℓ states. Since the *nd* states have a quantum defect (mod 1) of -0.25, we expect that fields approaching the Inglis-Teller field should be required to enhance DR, and in fact, this is the case experimentally [22,23]. Furthermore, for a given value of n, the E field enhancement saturates rapidly, since complete Stark mixing occurs for E fields not much larger than the Inglis-Teller field. In sum, the enhancement occurs for $E>E_{\mathrm{IT}}$, unlike the storage-ring experiments in which $E\ll E_{\mathrm{IT}}$. Consequently, in our experiments there is considerable n mixing of the Stark wave functions, due to the finite sized Ba core, but this effect is essentially absent in the storage-ring experiments.

Adding a B field perpendicular to the E field couples the m and $m\pm1$ states, which can lead to m mixing and an increase in the DR rate, as first pointed out by Robicheaux and Pindzola. However, it is not so immediately apparent why the B field should diminish the DR rate, as observed in the storage-ring experiments. A model used to describe atoms in a circularly polarized microwave E field gives reasonable insight into this problem [29]. This model is based on hydrogen and the assumption that the B field is weak enough such that there is no ℓ mixing, i.e., no diamagnetism. These restrictions correspond to the regime considered by Robicheaux and Pindzola.

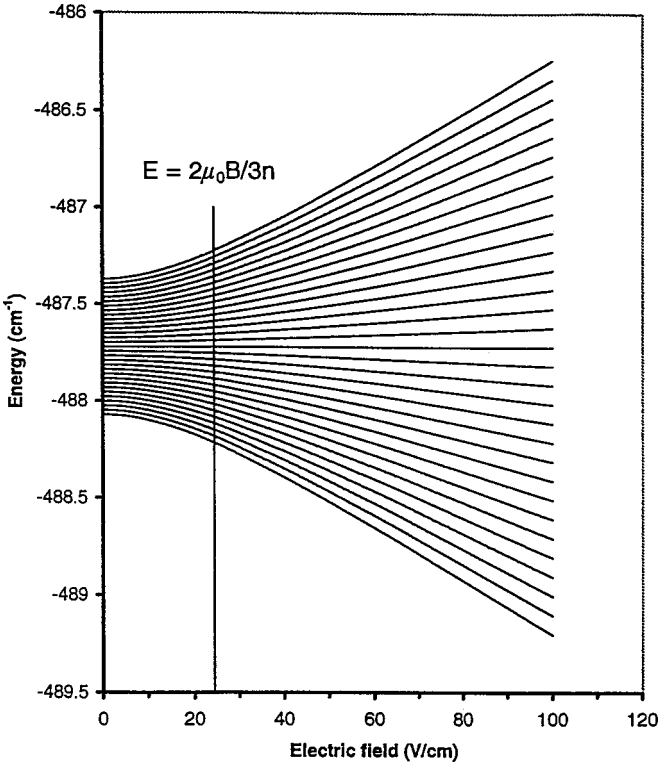

FIG. 11. Energy levels for $\vec{B}\perp\vec{E}$ [Eq. (7)] and $n=15$, $B=500$ G. The vertical line marks the electric field where the electric and magnetic interactions are comparable.

We begin by reversing the order in which we conceptually apply the fields, i.e., imagine that there is a nonzero B field in the z direction and that a variable perpendicular E field in the x direction is added. When $E=0$, the B field leads to a linear energy shift of $-m\mu_0B$, where μ_0 is the Bohr magneton, and the eigenstates are the ℓm states. At the other extreme of a high electric field the magnetic field is insignificant, and the energy eigenstates are the Stark states, for which the logical quantization axis is the x axis. To represent the energy levels at all E fields, we can use the expression [29]

$$W=-\frac{1}{2n^2}+k\sqrt{(\mu_0B)^2+\left(\frac{3nE}{2Z}\right)^2}, \qquad (11)$$

where k is an integer such that $-n\leqslant k\leqslant n$ and Z is the charge of the ion. In zero E field, k is the magnetic quantum number, with the z axis as the quantization axis and in high E field, k is the Stark quantum number, with the x axis as the quantization axis. States of $|k|<n$ are degenerate, and there is a high degeneracy of states for which $k\sim0$. The transition from magnetic to electric field dominance is shown in Fig. 11, a plot of the energies of Eq. (11) as a function of E for $n=15$ and $B=500$ G.

From Eq. (11) and Fig. 11, it is apparent that there is a transition from magnetic field dominance to electric field dominance when

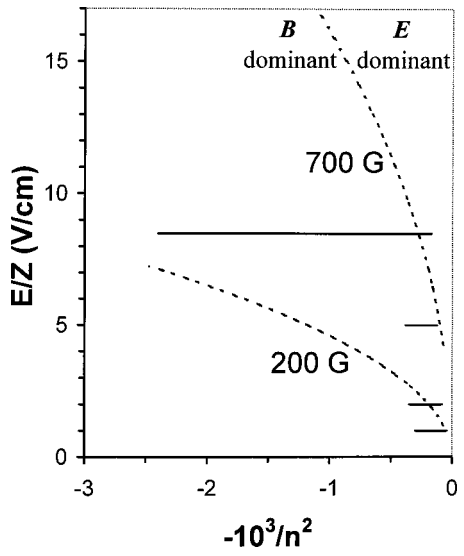

FIG. 12. Electric and magnetic field equivalence condition of Eq. (12) plotted vs $-10^3/n^2$, for $B=200$ and 700 G (-----). Above and to the right of the curve the E field is dominant and below and to the left the B field is dominant. In the region near the curve both E and B fields are important. The horizontal lines show the ranges of $-10^3/n^2$ covered in these experiments ($E/Z \leqslant 5$ V/cm) and in those of Bartsch *et al.* ($E/Z=8.5$ V/cm).

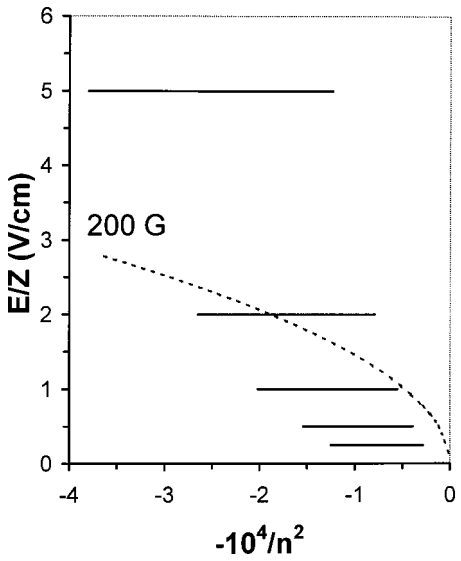

FIG. 13. Electric and magnetic field equivalence condition of Eq. (12) plotted vs $-10^4/n^2$, for $B=200$ G (-----). The horizontal lines show the ranges of $-10^4/n^2$ covered by our experiments. Note the change of abscissa relative to Fig. 12 by a factor of 10.

$$\mu_0 B = \frac{3nE}{2Z}, \tag{12}$$

or, for a given B, when

$$E = \frac{2\mu_0 BZ}{3n}. \tag{13}$$

When the condition of Eqs. (12) and (13) is met the eigenstates no longer have a well defined m, so there exists not only ℓ mixing as in a pure electric field but m mixing as well. Consequently, it is in this region that we expect to find the maximal enhancement of the DR rate. We would expect the maximum to be broad because the coupling strength due to the weaker field becomes stronger away from the condition of Eqs. (12) and (13). Explicitly, in the strong B limit the coupling due to the perpendicular E field scales as n^2E and in the strong E limit the coupling due to the perpendicular B field scales as $n\mu_0 B$. Each of these couplings has a factor of n not present in the radical of Eq. (11).

In Fig. 12, we show Eq. (13) for $B=200$ and 700 G plotted vs $-10^3/n^2$, which is proportional to the binding energy. Along the bold lines, the E and B fields are comparable and DR should be maximal. Above and to the right of the curve is the strong E limit, which should resemble the case in which there is only an E field. Below and to the left of the curve should resemble the case in which there is only a B field, which is equivalent to $B=0$ (and $E=0$). For a constant E, as B is increased from zero, we pass from the strong E limit to the regime in which the E and B fields are comparable and then to the strong B limit. Correspondingly, as B is increased from zero, we expect to see a rise to a maximum in the DR rate at the condition specified by Eqs. (12) and (13), followed by a decline. This expectation was also pointed out by Robicheaux and Pindzola [15]. In fact, we expect the DR rate to decrease to the $E=0$, $B=0$ rate at high magnetic fields.

We can use Fig. 12 to compare the storage-ring data and our data to the model. In the experiment of Bartsch *et al.* [18] with Cl^{14+} the maximum E field is 120 V/cm ($E/Z=8.57$ V/cm), and the enhancement occurs for $23 \leqslant n \leqslant 79$ with a peak at $n \sim 70$. For these values of n and $E=120$ V/cm, the spacings between m and $m \pm 1$ states, $3nE/2Z$, are 0.37 and 1.28 GHz, corresponding to B fields of 270 and 910 G. The range $20 \leqslant n \leqslant 79$ is shown in Fig. 12. For 200 G, it is clear that most of this range is in the strong E limit, while for 700 G most of it is in the strong B limit in which the electric-field enhancement is suppressed. Consequently, it is not surprising that the DR rate is decreasing with B near 700 G, but, based on our model, we would have expected a maximum at $B \sim 300-400$ G, not a monotonic decrease with B as was observed.

Our DR data were taken in E fields of up to 5 V/cm and B fields of up to 240 G, and in Fig. 13, we have shown the ranges covered for E fields from 0.25 to 5 V/cm. For the low E fields, our B field range spans the entire low B (strong E) to high B range. However, for the high E fields, we are always in the low B limit. The energy integrated data shown in Fig. 9 are in reasonable agreement with our expectations. For $E=\leqslant 1$ V/cm we can see a maximum in the enhancement as B is increased, for $E=5$ V/cm it is clear that there is no maximum, and for $E \geqslant 2$ V/cm the enhancement appears to just reach a maximum. On the other hand, if we take a closer look at the raw energy resolved data, shown in Figs. 3–8 we see some clear disagreements. For very high n, we are always in the strong E (weak B) limit, and the enhancement should appear first at lower n. Indeed, for $E \leqslant 1$ V/cm, it does, but for $E=2$ V/cm and 5 V/cm the enhancement ap-

pears simultaneously for all n. Furthermore, we would expect the B field enhancement to decrease at high n, but it is evident that it never does.

This simple model is physically appealing, and while it gives a reasonable description of the storage-ring experiments, there are obvious discrepancies with our experiment. In the storage-ring experiments of Bartsch *et al.* [18], the applied fields are always well below the Inglis-Teller field, so there are never overlapping n states. In contrast, in our experiments $E > E_{\mathrm{IT}}$, so the experiments are always in the regime in which there are overlapping Stark manifolds of different n. Since Ba is not at all hydrogenic, the overlapping Stark manifolds are coupled, and it is not obvious that the E field can ever dominate the B field in the clean way depicted in Fig. 12. In the $E > E_{\mathrm{IT}}$ regime, there are two important nonhydrogenic effects. First, the average spacing between states of m and $m \pm 1$ is not $3nE/2Z$ but $Z^2/2n^4$, so the levels are closer together than in a hydrogenic picture. This effect may effectively reduce the electric field. Second, the n levels are mixed, which allows magnetic dipole coupling between them. There is no magnetic dipole coupling between n states in a pure coulomb potential. While these nonhydrogenic effects may not be the entire reason for thediscrepancies between the model and the experiment, they are certainly important.

V. CONCLUSION

We have presented the results of an extensive study of DR from a CFB in Ba atoms in combined electric and magnetic fields, showing the predicted enhancement of DR in crossed B and E fields. Within experimental uncertainty, no enhancement was observed for $\vec{B} \| \vec{E}$, also in accordance with the prediction [13]. A simple model provides a qualitative understanding of the magnetic-field enhancement of DR and an explanation for the decrease of DR in the storage-ring experiments, but it does not reproduce all features of our experiments. Two natural extensions of this experiment are to increase the magnetic field ($\geqslant$700 G) to observe unambiguously a decrease of the DR enhancement as B is increased and to use an entrance channel with a smaller quantum defect to make contact with the storage-ring experiments.

ACKNOWLEDGMENTS

It is a pleasure to acknowledge stimulating discussions with R. R. Jones. This work had been supported by the U.S. Department of Energy.

[1] H. S. W. Massey and D. R. Bates, Rep. Prog. Phys. **9**, 62 (1942).
[2] A. Burgess, Astrophys. J. **139**, 776 (1964).
[3] A. Burgess and H. P. Summers, Astrophys. J. **157**, 1007 (1969).
[4] V. L. Jacobs, J. Davis, and P. C. Kepple, Phys. Rev. Lett. **37**, 1390 (1976).
[5] D. S. Belić, G. H. Dunn, T. J. Morgan, D. W. Mueller, and C. Timmer, Phys. Rev. Lett. **50**, 339 (1983).
[6] K. LaGattuta and Y. Hahn, Phys. Rev. Lett. **51**, 558 (1983).
[7] A. Müller, D. S. Belić, B. D. DePaola, N. Djurić, G. H. Dunn, D. W. Mueller, and C. Timmer, Phys. Rev. Lett. **56**, 127 (1986).
[8] T. Bartsch, A. Müller, W. Spies, J. Linkemann, H. Danared, D. R. DeWitt, H. Gao, Z. Wong, R. Schuch, A. Wolf, G. H. Dunn, M. S. Pindzola, and D. C. Griffin, Phys. Rev. Lett. **79**, 2233 (1997).
[9] V. L. Jacobs and J. Davis, Phys. Rev. A **19**, 776 (1979).
[10] K. A. Safinya, J. F. Delpech, and T. F. Gallagher, Phys. Rev. A **22**, 1062 (1980).
[11] S. M. Jaffe, R. Kachru, N. H. Tran, H. B. van Linden van den Heuvell, and T. F. Gallagher, Phys. Rev. A **30**, 1828 (1984).
[12] W. Huber and C. Bottcher, J. Phys. B **13**, L399 (1980).
[13] P. F. Dittner, S. Datz, P. D. Miller, P. L. Pepmiller, and C. M. Fou, Phys. Rev. A **35**, 3668 (1987).
[14] D. W. Savin, L. D. Gardner, D. B. Reisenfeld, A. R. Young, and J. L. Kohl, Phys. Rev. A **53**, 280 (1996).
[15] F. Robicheaux and M. S. Pindzola, Phys. Rev. Lett. **79**, 2237 (1997).
[16] D. C. Griffin, F. Robicheaux, and M. S. Pindzola, Phys. Rev. A **57**, 2708 (1998).
[17] K. LaGattuta and B. Borca, J. Phys. B **31**, 4781 (1998).
[18] T. Bartsch, S. Schippers, A. Müller, C. Brandau, G. Gwinner, A. A. Saghiri, M. Beutelspacher, M. Grieser, D. Schwalm, A. Wolf, H. Danared, and G. H. Dunn, Phys. Rev. Lett. **82**, 3779 (1999).
[19] T. Bartsch, S. Schippers, M. Beutelspacher, S. Böhm, M. Grieser, G. Gwinner, A. A. Saghiri, G. Saathoff, R. Schuch, D. Schwalm, A. Wolf, and A. Müller, J. Phys. B **33**, L453 (2000).
[20] V. Klimenko, L. Ko, and T. F. Gallagher, Phys. Rev. Lett. **83**, 3808 (1999).
[21] J. P. Connerade, Proc. R. Soc. London, Ser. A **362**, 361 (1978).
[22] J. G. Story, B. J. Lyons, and T. F. Gallagher, Phys. Rev. A **51**, 2156 (1995).
[23] L. Ko, V. Klimenko, and T. F. Gallagher, Phys. Rev. A **59**, 2126 (1999).
[24] T. F. Gallagher, *Rydberg Atoms* (Cambridge University Press, Cambridge, 1994).
[25] M. G. Littman, Proc. SPIE **912**, 56 (1988).
[26] C. E. Moore, *Atomic Energy Levels*, Natl. Bur. Stand. (U.S.) Circ. No. 467 (U.S. GPO, Washington, D.C., 1949).
[27] T. Bartsch, A. Müller, W. Spies, J. Linkemann, H. Danared, D. R. Dewitt, H. Gao, W. Zong, R. Schuch, A. Wolf, G. H. Dunn, M. S. Pindzola, and D. C. Griffin, Phys. Rev. Lett. **79**, 2233 (1997).
[28] C. Brandau, T. Bartsch, A. Hoffnecht, H. Knopp, S. Schippers, W. Shi, A. Muller, N. Grun, W. Scheid, T. Steih, F. Bosch, B. Franzke, C. Kozhuharov, P. H. Mokler, F. Nolden, M. Steck, T. Stohlker, and Z. Stachum, Phys. Rev. Lett. **89**, 053201 (2002).
[29] D. Wintgen, Z. Phys. D: At., Mol. Clusters **18**, 125 (1991).